

Search for Dark Particles in $K_L^0 \rightarrow \gamma X$ at the KOTO Experiment

T. Wu,¹ Y. C. Tung,² Y. B. Hsiung,¹ J. K. Ahn,³ M. Gonzalez,^{4,*} E. J. Kim,⁵ T. K. Komatsubara,^{6,7} K. Kotera,⁴ S. K. Lee,⁵ G. Y. Lim,^{6,7} C. Lin,⁸ T. Matsumura,⁹ H. Nanjo,⁴ Y. Noichi,⁴ T. Nomura,^{6,7} T. Nunes,⁴ K. Ono,⁴ J. Redeker,¹⁰ N. Shimizu,^{4,†} S. Shinohara,^{4,‡} K. Shiomi,^{6,7} R. Shiraiishi,^{4,‡} Y. Tajima,¹¹ Y. W. Wah,¹⁰ H. Watanabe,^{6,7} T. Yamanaka,⁴ and H. Y. Yoshida¹¹

(KOTO Collaboration)

¹Department of Physics, National Taiwan University, Taipei 10617, Taiwan, Republic of China

²Department of Physics, National Kaohsiung Normal University, Kaohsiung 824, Taiwan

³Department of Physics, Korea University, Seoul 02841, Republic of Korea

⁴Department of Physics, Osaka University, Toyonaka, Osaka 560-0043, Japan

⁵Division of Science Education, Jeonbuk National University, Jeonju 54896, Republic of Korea

⁶Institute of Particle and Nuclear Studies, High Energy Accelerator

Research Organization (KEK), Tsukuba, Ibaraki 305-0801, Japan

⁷J-PARC Center, Tokai, Ibaraki 319-1195, Japan

⁸Department of Physics, National Changhua University of Education, Changhua 50007, Taiwan

⁹Department of Applied Physics, National Defense Academy, Kanagawa 239-8686, Japan

¹⁰Enrico Fermi Institute, University of Chicago, Chicago, Illinois 60637, USA

¹¹Department of Physics, Yamagata University, Yamagata 990-8560, Japan

We report a search for an invisible particle X in the decay $K_L^0 \rightarrow \gamma X$ ($X \rightarrow$ invisible), where X can be interpreted as a massless or massive dark photon. No evidence for X was found, based on 13 candidate events consistent with a predicted background of $12.66 \pm 4.42_{\text{stat.}} \pm 2.13_{\text{syst.}}$ events. Upper limits on the branching ratio of $K_L^0 \rightarrow \gamma X$ were set for the X mass range $0 \leq m_X \leq 425 \text{ MeV}/c^2$. For massless X , the upper limit was 3.4×10^{-7} at the 90% confidence level, while for massive X , the upper limits in the searched mass region ranged from $\mathcal{O}(10^{-7})$ to $\mathcal{O}(10^{-3})$.

Introduction The KOTO experiment at J-PARC [1] was designed for a dedicated search for the rare decay $K_L^0 \rightarrow \pi^0 \nu \bar{\nu}$, a process that is challenging to identify due to the lack of kinematic constraints. To meet this challenge, together with the intense proton beam at J-PARC that provides a large number of kaons, KOTO employs a hermetic veto system with exceptional background-rejection capability. These features have enabled KOTO to set the current world's best upper limit on the branching ratio of $K_L^0 \rightarrow \pi^0 \nu \bar{\nu}$ [2]. The same experimental environment also provides a powerful opportunity to explore physics beyond the Standard Model (SM), including searches for hidden particles [2][3].

Here, we present a search for a hidden particle X in the decay $K_L^0 \rightarrow \gamma X$, where X can be interpreted as a dark photon, the gauge boson of a new Abelian symmetry $U(1)_D$ invoked in extensions of the SM with dark sectors [4][5]. We probed the mass range of X from 0 to $425 \text{ MeV}/c^2$, under the assumption that X decays invisibly. This region covers two theoretical scenarios: a massive dark photon (A') arising from a spontaneously broken $U(1)_D$, or a massless dark photon ($\bar{\gamma}$) if the symmetry remains unbroken. In the massive case, A' could couple to the SM particles through kinetic mixing, and the decay $K_L^0 \rightarrow \gamma A'$ was discussed in [6]. In the unbroken case, $\bar{\gamma}$ can only couple to SM particles through higher-dimensional operators. Nevertheless, an estimate suggested that the branching ratio of $K_L^0 \rightarrow \gamma \bar{\gamma}$ could be as large as 1.2×10^{-3} [7], which is within the experimental reach of KOTO.

KOTO apparatus Neutral kaons are produced by 30-GeV protons from the J-PARC Main Ring incident on a gold target [8] and are extracted at 16° to the proton beam using two collimators with a sweeping magnet between them [9]. The resulting neutral beam, consisting mainly of K_L^0 s, neutrons, and photons, has a K_L^0 momentum distribution peaking at $1.4 \text{ GeV}/c$, a solid angle of 7.8 psr , and a transverse size of $8 \times 8 \text{ cm}^2$ at the exit of the downstream collimator. The K_L^0 s are transported to the KOTO detector located 21.5 m downstream of the target.

Figure 1 shows a cross-sectional view of the KOTO detector, with the coordinate origin defined on the beam axis at the detector entrance. At the downstream end of the decay volume ($z \approx 6.1 \text{ m}$), the CsI calorimeter (CSI) measures the energy and position of photons from the $K_L^0 \rightarrow \gamma X$ decay [10]. It is composed of 2716 undoped cesium iodide crystals arranged in a cylindrical shape of 95 cm radius with a central 200-mm square beam hole.

The remaining detector components serve as veto counters for particles escaping CSI. The Main Barrel (MB), Inner Barrel (IB), and Front Barrel (FB) are lead-scintillator sandwich detectors arranged cylindrically around the decay volume. Along the beamline, the Collar Counters (NCC and CC03–CC06) surround the beam, forming a series of vetoes for particles escaping in the beam direction. The Outer Edge Veto (OEV) and CC03, covering the outer and inner surfaces of CSI, respectively, measure energy leakage to ensure full energy containment within CSI. Dedicated charged-particle ve-

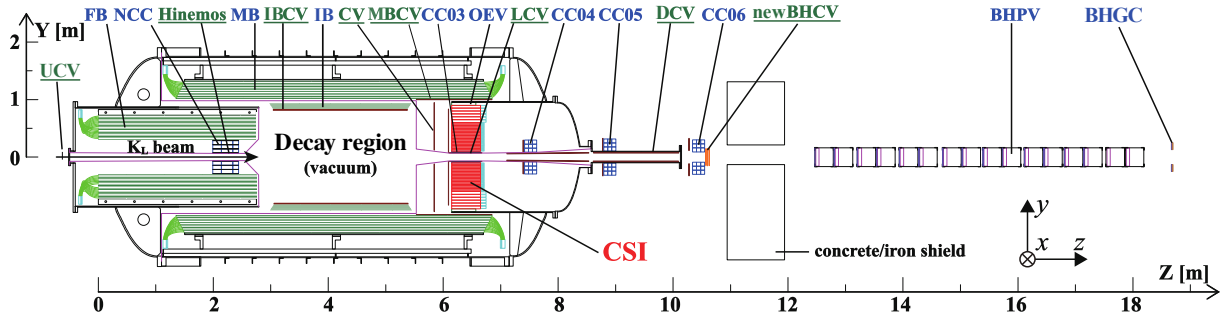


FIG. 1. Cross-sectional view of the KOTO detector, with the beam entering from the left. The detector components with their names underlined represent charged-particle veto counters. The other components, except for CSI, serve as photon veto counters.

toes are placed in front of CSI (CV), in the innermost layers of MB and IB (MBCV and IBCV), and along the beam pipe (LCV, DCV). In the downstream beamline, the BHPV and newBHCV detectors identify in-beam photons and charged particles, respectively.

Analog pulses from all detector channels are digitized and recorded individually. CSI channels use custom 125-MHz ADC modules [11], while veto channels are digitized with either 125-MHz or 500-MHz modules.

Data collection For this analysis, data was collected during a dedicated 2-hour run in June 2020. With the J-PARC accelerator operating at 51 kW, a total of 5.03×10^{16} protons on target (POT) were delivered, producing $1.29 \times 10^{10} K_L^0$ decays at the exit of the K_L^0 beam line. Events for the $K_L^0 \rightarrow \gamma X$ search were selected online using a two-level trigger system. The Level-1 (L1) trigger required the total energy in CSI to exceed 300 MeV with no coincident activity in the CV, IB, MB, NCC, or CC03–CC06 veto detectors. The Level-2 (L2) trigger further required exactly one photon in CSI. To study trigger effects and determine the K_L^0 flux, an additional trigger with looser L1 veto conditions and no L2 selection was simultaneously employed with a prescale factor of 13.

Separate neutron runs were conducted to collect beam neutron events for studying the neutron background in the $K_L^0 \rightarrow \gamma X$ analysis. During the neutron run, a 3-mm-thick aluminum plate was inserted into the beam at 669 mm upstream of the detector entrance to scatter neutrons and enhance their interactions with CSI. These events were collected with the same L1 veto requirements as for $K_L^0 \rightarrow \gamma X$, but with the L2 condition requiring two clusters in CSI for cleaner neutron samples, since one-cluster neutron data was contaminated by $K_L^0 \rightarrow \gamma\gamma$ decays with a missing photon due to veto inefficiency. The two clusters in a neutron event typically arose from multiple hadronic interactions of a single neutron at separate locations within CSI. Contamination from $K_L^0 \rightarrow \gamma\gamma$ events in the two-cluster sample was greatly suppressed by excluding events in which the center-of-energy of the two clusters was near the center of CSI and the opening

angle between the position vectors of the two clusters on the CSI surface plane was close to 180° .

Event reconstruction and selection The particle X and its decay products were assumed to be non-interacting with the KOTO detector; therefore, a $K_L^0 \rightarrow \gamma X$ event was characterized by a single photon in CSI with no coincident activity in any veto detector. The cluster produced by photon interactions in CSI was reconstructed by grouping neighboring crystals with energy deposits above 3 MeV within a 150-ns time window. The resulting cluster provided measurements of the photon's energy (E_γ) and position (x, y) on the upstream surface of CSI. To ensure full containment of the photon's energy, the cluster position was required to lie within the fiducial region defined by $H_{XY} > 175$ mm and $\sqrt{x^2 + y^2} < 850$ mm, where H_{XY} denoted the larger of $|x|$ or $|y|$. The lower bound on H_{XY} also suppressed backgrounds from upstream kaon decays, in which a kaon decayed before entering the detector and one of its decay products hit the inner edge of CSI. The photon energy was required to exceed 500 MeV. The signal region was further defined by requiring $900 < E_\gamma < 3000$ MeV and $325 < H_{XY} < 850$ mm. The broader region, $800 < E_\gamma < 3000$ MeV and $300 < H_{XY} < 850$ mm, which marginally covered the signal region to avoid edge-tuning bias, was kept blinded until all event selection criteria were finalized.

To ensure that no particles were present other than a single photon in CSI, events were discarded if in-time energy deposits in the veto detectors exceeded the following thresholds: 1 MeV for FB, MB, IB, NCC, MBCV, IBCV, and OEV; 3 MeV for CC03–CC06; and 0.2 MeV for CV; Furthermore, BHPV was required to have less than three consecutive modules with in-time energy deposits.

Background suppression Backgrounds for $K_L^0 \rightarrow \gamma X$ were classified into two main categories: neutron- and kaon-induced sources. The neutron-induced background was evaluated using data collected during dedicated neutron runs. Contributions from various K_L^0 decay channels were estimated using GEANT4-based Monte Carlo (MC) simulations [12][13]. The MC was further over-

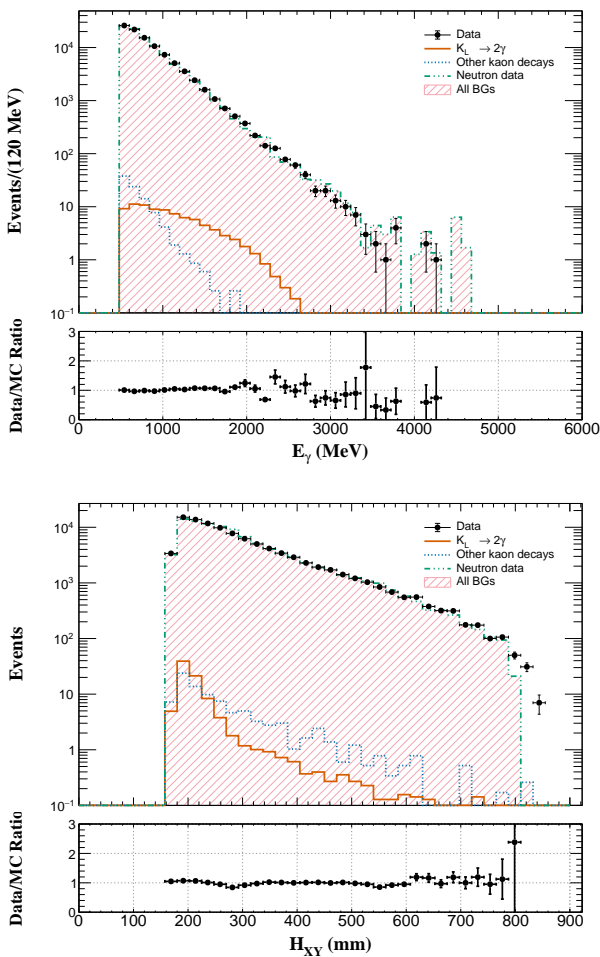


FIG. 2. Distributions of E_γ and H_{XY} after requiring no in-time signal in veto counters. Black dots represent the data, while the hollow histograms show the contributions from each background source indicated in the figure. “Other kaon decays” include all K_L^0 backgrounds summarized in Table I, excluding $K_L^0 \rightarrow \gamma\gamma$. The neutron data corresponds to samples collected in dedicated neutron runs. The shaded histogram represents the sum of all backgrounds.

laid with accidental data collected simultaneously with physics data to reproduce actual beam activity and random electronic noise. The agreement between the data and the modeled background spectra is shown in Figure 2.

Beam neutrons that scatter into CsI and produce one photon-like cluster were the dominant background in this analysis. This background was studied using two-cluster events collected during dedicated neutron runs, where the higher-energy cluster, typically produced by the neutron’s initial interaction in CsI, was selected to model the neutron background in $K_L^0 \rightarrow \gamma X$. The selected neutron cluster was normalized to the $K_L^0 \rightarrow \gamma X$ data using events identified as neutron-like by their cluster shapes (as described below) in the region $800 < E_\gamma < 3000$ MeV

and $175 < H_{XY} < 300$ mm. To account for differences in neutron cluster positions between two-cluster neutron data and one-cluster $K_L^0 \rightarrow \gamma X$ data, the H_{XY} distribution of the selected neutron cluster was weighted to match that of the $K_L^0 \rightarrow \gamma X$ data after normalization.

The neutron background was suppressed using three techniques: Cluster Shape Discrimination (CSD), Pulse Shape Discrimination (PSD), and Shower Depth Measurement (SDM). CSD distinguished neutrons from photons based on differences in the cluster patterns produced by hadronic interactions of neutrons and electromagnetic interactions of photons. PSD exploited differences in the pulse shapes recorded in individual CsI channels to discriminate neutrons from photons. Further details of CSD and PSD are given in [14]. SDM measured the shower depth along the z -direction in CsI by evaluating the pulse timing difference (ΔT) between the upstream MPPC and downstream PMT at the two ends of each CsI crystal. Photon-induced electromagnetic showers typically developed near the upstream surface, whereas neutron-induced hadronic interactions could occur more uniformly throughout the crystal, as the interaction length of CsI is approximately 20 times larger than its radiation length. Figure 3 shows the distributions of ΔT for the photon and neutron samples. By combining these three techniques, the neutron background was suppressed by a factor of 560, resulting in $11.57 \pm 4.42_{\text{stat.}} \pm 2.13_{\text{syst.}}$ events in the signal region. The statistical uncertainty was dominated by the limited statistics of the neutron data sample, while the systematic uncertainty, estimated using neutron-like events for normalization, accounted for discrepancies in individual selection criteria (cuts) between $K_L^0 \rightarrow \gamma X$ and neutron data.

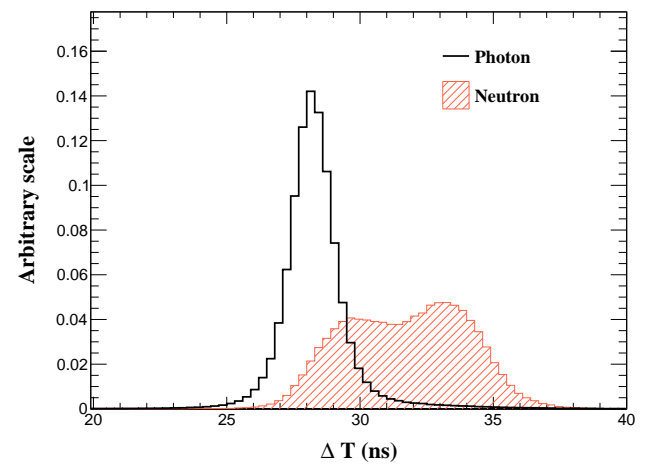


FIG. 3. Distributions of ΔT . The hollow histogram shows the photon sample from $K_L^0 \rightarrow \pi^0 \pi^0 \pi^0$ data, while the shaded histogram represents the neutron sample from dedicated neutron runs.

TABLE I. Summary of background estimation.

Source	Number of events
K_L^0 decay	
$K_L^0 \rightarrow \gamma\gamma$	$1.09 \pm 0.12_{\text{stat.}} \pm 0.05_{\text{syst.}}$
$K_L^0 \rightarrow \pi^0\pi^0\pi^0$	< 0.18 (90% C.L.)
$K_L^0 \rightarrow \pi^0\pi^0$	< 0.05 (90% C.L.)
$K_L^0 \rightarrow \pi^\pm e^\mp \nu_e$	< 0.27 (90% C.L.)
$K_L^0 \rightarrow \pi^\pm \mu^\mp \nu_\mu$	< 0.25 (90% C.L.)
$K_L^0 \rightarrow \pi^+\pi^-\pi^0$	< 0.17 (90% C.L.)
Neutron	$11.57 \pm 4.42_{\text{stat.}} \pm 2.13_{\text{syst.}}$
Total (central value)	$12.66 \pm 4.42_{\text{stat.}} \pm 2.13_{\text{syst.}}$

The $K_L^0 \rightarrow \gamma\gamma$ decay was the most dominant background among all K_L^0 decays, as it shares a similar phase space with $K_L^0 \rightarrow \gamma X$ and could mimic the signal if one of the final-state photons escaped detection. After applying all selection criteria, the number of $K_L^0 \rightarrow \gamma\gamma$ background events in the signal region was estimated to be $1.09 \pm 0.12_{\text{stat.}} \pm 0.05_{\text{syst.}}$. The systematic uncertainty was evaluated using two-cluster $K_L^0 \rightarrow \gamma\gamma$ data and MC events, in which one of the two photons was randomly selected to compare their differences. Backgrounds from other K_L^0 decay channels are summarized in Table I. Combining all background sources, the total number of background events in the signal region was evaluated to be $12.66 \pm 4.42_{\text{stat.}} \pm 2.13_{\text{syst.}}$.

Single event sensitivity and systematic uncertainties The Single Event Sensitivity (SES) was defined as the branching ratio corresponding to the observation of one signal event and was calculated as

$$SES = \frac{A_{\text{norm}}}{A_{\text{sig}}} \times \frac{1}{N_{\text{norm}}} \times \mathcal{B}_{\text{norm}}, \quad (1)$$

where A_{norm} , N_{norm} , and $\mathcal{B}_{\text{norm}}$ denoted the acceptance, the number of observed events, and the nominal branching ratio of $K_L^0 \rightarrow \pi^0\pi^0\pi^0$ from [15], respectively. From these quantities, the K_L^0 flux was obtained as $N_{\text{norm}}/(A_{\text{norm}} \times \mathcal{B}_{\text{norm}}) = (1.29 \pm 0.02) \times 10^{10}$, with N_{norm} corrected for the online trigger prescale factor. The signal acceptance A_{sig} , which includes the K_L^0 decay probability within the KOTO detector, was obtained from the $K_L^0 \rightarrow \gamma X$ MC simulation and evaluated to be $(2.697 \pm 0.002) \times 10^{-3}$ for massless X , yielding an SES of $(2.87 \pm 0.05_{\text{stat.}} \pm 0.30_{\text{syst.}}) \times 10^{-8}$. For massive X , the sensitivity becomes worse with increasing X mass due to lower E_γ , causing events to fall below the 900-MeV lower bound of the signal region.

Table II summarizes the systematic uncertainties in the SES calculation arising from (a) the veto cuts, (b) the kinematic cuts for $K_L^0 \rightarrow \pi^0\pi^0\pi^0$, (c) the kinematic cuts for $K_L^0 \rightarrow \gamma X$, (d) the neutron cuts for $K_L^0 \rightarrow \gamma X$, (e) the K_L^0 momentum spectrum, (f) the trigger effects, and (g) Branching ratio of $K_L^0 \rightarrow \pi^0\pi^0\pi^0$. Uncertainties (a), (b), and (c) were derived from discrepancies in acceptance between data and MC for individual selection cuts, with percentage differences combined in quadrature. The

dominant contribution came from source (a) (6.6%). For $K_L^0 \rightarrow \pi^0\pi^0\pi^0$, the uncertainty was obtained by direct comparison of data and MC, while for $K_L^0 \rightarrow \gamma X$ it was evaluated from differences in the photon spectrum of $K_L^0 \rightarrow \gamma\gamma$ data and MC. The uncertainty (d) accounted for the photon acceptance of the aforementioned three neutron-selection cuts and was estimated similarly from comparisons between photons in $K_L^0 \rightarrow \gamma\gamma$ data and MC. The uncertainty (e) was estimated from the difference between the K_L^0 momentum spectra in data and MC. The trigger-related uncertainty (f) was evaluated using data samples collected with looser L1 cuts and without L2 selections. The uncertainty (g) in the branching ratio of $K_L^0 \rightarrow \pi^0\pi^0\pi^0$ was taken from [15].

TABLE II. Summary of Systematic Uncertainties in SES.

Sources	Uncertainty
(a) Veto cuts	6.6%
(b) Kinematic cuts for $K_L^0 \rightarrow \pi^0\pi^0\pi^0$	3.3%
(c) Kinematic cuts for $K_L^0 \rightarrow \gamma X$	1.4%
(d) Neutron cuts for $K_L^0 \rightarrow \gamma X$	4.8%
(e) K_L^0 momentum spectrum	0.9%
(f) Trigger effect	1.6%
(g) Branching ratio of $K_L^0 \rightarrow \pi^0\pi^0\pi^0$	0.6%
Total	9.1%

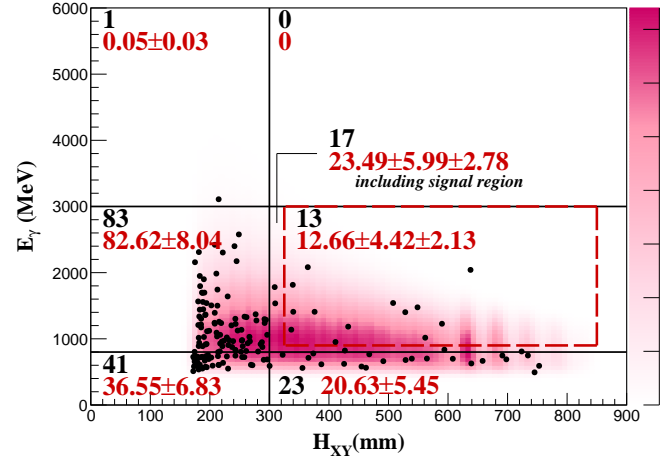


FIG. 4. Distribution of E_γ versus H_{XY} after all selection criteria for $K_L^0 \rightarrow \gamma X$. The red rectangle indicates the signal region. Black dots are the observed events, and the shaded contour shows the $K_L^0 \rightarrow \gamma X$ MC distribution for massless X . Numbers in black (red) represent the observed (expected) event counts.

Conclusions After finalizing the selection criteria, the signal region was unblinded, revealing 13 events in the signal region, as shown in Figure 4. This observation was consistent with the expected background of $12.66 \pm 4.42_{\text{stat.}} \pm 2.13_{\text{syst.}}$, and no evidence for $K_L^0 \rightarrow \gamma X$ was found. With the uncertainties in the background es-

timation incorporated, an upper limit on the number of $K_L^0 \rightarrow \gamma X$ candidates at the 90% confidence level (C.L.) was determined to be 11.9 events using the Feldman-Cousins method [16]. Upper limits on the branching ratio of $K_L^0 \rightarrow \gamma X$ were derived for different masses of X in the range 0–425 MeV/ c^2 . For massless X , the upper limit on the branching ratio was set to be 3.4×10^{-7} at the 90% C.L., while for massive X , the 90% C.L. upper limits ranged from 3.4×10^{-7} at $m_X = 25$ MeV/ c^2 to 8.0×10^{-3} at $m_X = 425$ MeV/ c^2 , as shown in Figure 5.

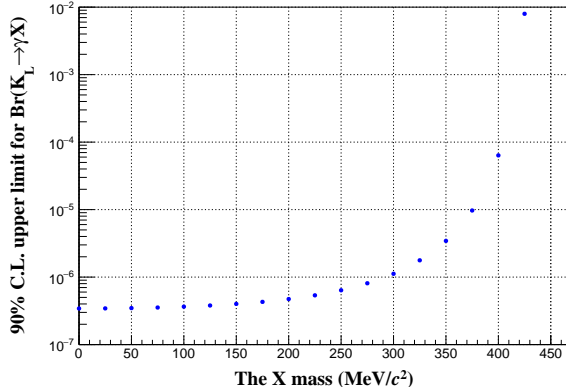


FIG. 5. Upper limit at the 90% C.L. on the branching fraction of the $K_L^0 \rightarrow \gamma X$ decay as a function of the X mass.

This analysis set upper limits on the branching ratio of $K_L^0 \rightarrow \gamma X$, a decay with minimal kinematic constraints, demonstrating KOTO’s precise understanding and control of its experimental environment. However, the sensitivity of this search was primarily limited by background levels. While collecting additional data could improve statistical uncertainties, significant improvements would require enhanced techniques for background suppression.

We thank Dr. Jusak Tandean for his valuable discussions and theoretical insights on this study. We would like to express our gratitude to all members of the J-PARC Accelerator and Hadron Experimental Facility groups for their support. We also thank the KEK Computing Research Center for KEKCC, the National Institute of Informatics for SINET4, and the University of Chicago Computational Institute for the GPU farm. This material is based upon work supported by the Ministry of Education, Culture, Sports, Science, and Technology (MEXT) of Japan and the Japan Society for the Promotion of Science (JSPS) under KAKENHI Grant Numbers JP16H06343 and JP21H04995 and

through the Japan-U.S. Cooperative Research Program in High Energy Physics; the U.S. Department of Energy, Office of Science, Office of High Energy Physics, under Awards No. DE-SC0009798; the National Science and Technology Council (NSTC) and Ministry of Education (MOE) in Taiwan, under Grant Numbers NSTC-108-2112-M-002-001, NSTC-109-2112-M-002-021, NSTC-109-2112-M-002-013, NSTC-110-2112-M-002-020, MOE-109L892105, and MOE-110L890205 through National Taiwan University; the National Research Foundation of Korea under Grant Numbers 2020R1A3B2079993, RS-2022-NR070836, and RS-2025-00556834.

* Present address: CERN, European Organization for Nuclear Research, CH-1211 Geneva, Switzerland.

† Present address: Department of Physics and The International Center for Hadron Astrophysics, Chiba University, Chiba 263-8522, Japan.

‡ Present address: Institute of Particle and Nuclear Studies, High Energy Accelerator Research Organization (KEK), Tsukuba, Ibaraki 305-0801, Japan.

- [1] S. Nagamiya, Prog. Theor. Exp. Phys. **02B001** (2012).
- [2] J. Ahn *et al.* (KOTO Collaboration), Phys. Rev. Lett. **134**, 081802 (2025).
- [3] C. Lin *et al.* (KOTO Collaboration), Phys. Rev. Lett. **130**, 111801 (2023).
- [4] M. Fabbrichesi, E. Gabrielli, and G. Lanfranchi, SpringerBriefs in Physics, 10.1007/978-3-030-62519-1 (2021).
- [5] B. A. Dobrescu, Phys. Rev. Lett. **94**, 151802 (2005).
- [6] J. F. Kamenik and C. Smith, J. High Energy Phys. **03**, 090 (2012).
- [7] J.-Y. Su and J. Tandean, Eur. Phys. J. C **80**, 824 (2020).
- [8] M. Saito *et al.*, Phys. Rev. Accel. Beams **25**, 063001 (2022).
- [9] T. Shimogawa, Nucl. Instrum. Methods Phys. Res., Sect. A **623**, 585 (2010).
- [10] K. Sato *et al.*, Nucl. Instrum. Methods Phys. Res., Sect. A **982**, 164527 (2020).
- [11] M. Bogdan, J. Genat, and Y. Wah, in *2007 IEEE Nuclear Science Symposium Conference Record*, Vol. 1 (IEEE, 2007) pp. 133–134.
- [12] J. Allison, K. Amako, J. Apostolakis, H. Araujo, P. Dubois *et al.* (GEANT4 Collaboration), IEEE Trans. Nucl. Sci **53**, 270 (2006).
- [13] S. Agostinelli *et al.* (GEANT4 Collaboration), Nucl. Instrum. Methods Phys. Res., Sect. A **506**, 250 (2003).
- [14] Y.-C. Tung *et al.*, Nucl. Instrum. Methods Phys. Res., Sect. A **1059**, 169010 (2024).
- [15] S. Navas *et al.* (Particle Data Group), Phys. Rev. D **110**, 030001 (2024).
- [16] G. J. Feldman and R. D. Cousins, Phys. Rev. D **57**, 3873 (1998).